Monitoring and Interpretation of Photoinduced Biochemical Processes by Rapid-Scan FTIR Difference Spectroscopy and Hybrid Hard and Soft Modeling

Lionel Blanchet,*[,†,‡] Cyril Ruckebusch,[†] Alberto Mezzetti,[†,§] Jean Pierre Huvenne,[†] and Anna de Juan[‡]

Laboratoire de Spectrochimie Infrarouge et Raman (LASIR), UMR CNRS 8516, Université des Sciences et Technologies de Lille (USTL), bât. C5, 59655 Villeneuve d'Ascq, France; Chemometrics Group, Department of Analytical Chemistry, Universitat de Barcelona, Diagonal, 647, 08028 Barcelona, Spain; and Service de Bioénenergétique Biologie Structurale et Mécanismes (SB2SM), iBiTecS, CEA, URA CNRS 2096, F-91191 Gif-sur-Yvette, France

Received: June 25, 2008; Revised Manuscript Received: February 12, 2009

Natural photochemical processes often require special instrumentation to monitor them at a suitable time scale. Rapid-scan FTIR difference spectroscopy is one of the preferred techniques to obtain rich structural information in the scale of milliseconds about photochemical processes of complex natural systems. The difference spectra obtained by this technique enhance the fine spectroscopic changes undergone during the process but require powerful data analysis methodologies to take full advantage of the information provided. Hybrid hard- and soft-modeling methodologies allow for coping with difficulties linked to the nature of the time-resolved measurement and to the complexity of the kinetic model describing the natural photochemical process. Thus, this methodology presents the following advantages: (a) handles difference spectra, taking into account the consequences of the lack of measurement about the initial stage of the process, (b) models events of the process that may be defined by a kinetic model (by hard modeling) and events that do not obey a mechanistic behavior (by soft modeling), (c) adapts to the photoaccumulation/relaxation stages of reversible photochemical processes, and (d) works simultaneously with series of experiments performed in different conditions and showing different kinetic behavior. The results of this data treatment provide complete kinetic information on the photochemical processes, e.g., rate constants, and a global picture of the difference spectra and the concentration profiles linked to each of the events (hard or soft modeled) contributing to the measured signal. The performance of the combination of time-resolved differential FTIR and hybrid hard and soft modeling is shown in a complex case study related to the photosynthetic activity of the reaction center of the purple bacteria *Rhodobacter sphaeroides.*

Introduction

Photoinduced processes are of particular interest in various fields of science, e.g., organic synthesis,[1] polymer science,[2] CMOS technology,[3] and biochemistry.[4] A comprehensive understanding of such processes relies on the use of advanced instrumentation, with time resolution ranging from the second to femtosecond time scale. Time-resolved FTIR techniques such as rapid scan[5] or step scan[6] fit the requirements of photochemistry and, as an additional advantage, provide spectra containing a lot of structural information (molecular vibrations depend on the chemical structure of the molecules as well as on their intra- and intermolecular interactions). Moreover, IR difference spectroscopy (performing successive differences between the current spectra and the spectrum measured before triggering) enhances the information linked to the molecular groups that have undergone a change because of the reaction. Such an aspect is particularly adapted to the investigation of photoinduced biochemical reactions, where the process usually takes place just in the active site of the protein, involving some specific amino acids and cofactors.[7] As we are dealing with light-induced reactions, these can be easily induced inside the IR cell, either by a laser flash[7] or by lamp illumination.[8] In the latter case, difference spectra are obtained by performing the subtraction between the spectra recorded under illumination and the initial spectrum recorded in the dark, so that photoaccumulation phenomena can be studied. This approach has been applied to investigate fast-decaying photobiological events.[9−11]

Classical kinetic analysis based on the study of single wavenumber traces has a limited performance to deal with these photochemical processes due to the spectroscopic overlap of coexisting evolving species and to the impossibility to detect interfering species in the signal measured. For this reason, more powerful multivariate chemometric methods are needed in order to improve the extraction of the chemical information that can be obtained from the data.

In the analysis of photochemical processes, the difference spectra obtained by rapid-scan FTIR are by themselves the first challenge. In fact, most of the chemometric algorithms are designed to deal with pure contributions that are directly associated with specific chemical species; i.e., a kinetic profile and a pure spectrum are expected for each chemical compound in a process. Conversely, in time-resolved infrared difference spectroscopy, as in rapid-scan difference FTIR, the pure contributions obtained are associated with events of the process; e.g., pure difference spectra show positive peaks corresponding

* To whom correspondence should be addressed. Tel.: +33 (0) 3 20 43 66 61. Fax: +33 (0) 3 20 43 67 55. E-mail: l.blanchet@science.ru.nl.
[†] Université des Sciences et Technologies de Lille.
[‡] Universitat de Barcelona.
[§] iBiTecS, CEA.

10.1021/jp8056042 CCC: $40.75
Published on Web 04/06/2009

to the formation of one or more products and negative peaks linked to the progressive disappearance of the related reactants. The absence of a direct correspondence chemical compound-modeled contribution comes from the lack of knowledge of the spectrum at the initial stage of the process. For a complete kinetic data analysis, these initial species should be taken into account and be treated as nonabsorbing species.[12]

Recently, soft-modeling multivariate curve resolution (MCR)[13,14] was applied to investigate photobiological reactions monitored by rapid-scan difference FTIR.[11,15] This kind of analysis was made without using any a priori knowledge on the kinetic model governing the process, and the resolution of the experimental spectra into a small number of contributions, defined by pure difference spectra and kinetic profiles, was obtained. Using this approach, relevant structural information could be obtained from the pure difference spectra and the kinetic evolution of the absorbing contributions could be interpreted. However, this soft-modeling methodology could not model the initial nonabsorbing species in difference spectroscopy and could not use the information of kinetic models in an explicit way.[12]

In contrast to soft-modeling methods, hard-modeling methods work postulating a kinetic model to explain the experimental variation of the spectroscopic measurements and, hence, are potentially well adapted to the study of time-resolved data. They allow for the introduction of nonabsorbing species in the models proposed and this is an advantage when dealing with difference spectra. However, hard-modeling approaches need a complete a priori knowledge of the evolution of the chemical system; i.e., they need to describe all the measured experimental variation by means of the selected kinetic model. This is a serious drawback when the knowledge of the kinetic behavior is incomplete and, particularly, when absorbing interferences not involved in the process are present.

The recently developed hybrid methodology hard−soft multivariate curve resolution (HS-MCR)[16] offers a solution to the shortcomings linked to pure hard- and soft-modeling approaches. Compared with pure soft modeling approaches, HS-MCR additionally provides estimates of the process parameters, i.e., rate constants,[16−18] and helps to minimize the ambiguity associated with the soft-modeling data decomposition.[13] As an improvement to pure hard-modeling methods, HS-MCR can model processes in the presence of absorbing interferences, since hard modeling is only applied to the species involved in the process and the interferences are left to be soft-modeled.[17,18] In common with hard-modeling methods, HS-MCR has been proven to be able to deal with the specific problems induced by difference spectra, by including nonabsorbing species to take into account the species at the initial stages of the process.[12] Because the basic scaffold of HS-MCR is the soft-modeling algorithm, the last relevant benefit is the flexibility in the analysis of multiple experiments, which can admit the application of different constraints and kinetic models to explain the spectral variation measured in the different experiments.

The aim of this work is to demonstrate the viability of the hard−soft-modeling method for the analysis of time-resolved rapid-scan FTIR difference spectra of photoinduced reactions, taking as a case study the chemical system of the reaction center (RC) placed in photosynthetic membranes of the purple bacterium *Rhodobacter sphaeroides*. This is a well-characterized system and a detailed knowledge of the relative position and orientation of cofactors and amino acids is available, as well as several pieces of information on its working mechanism.[19,20] In the past few years, an increasing amount of information has been gathered also on the structure of the photosynthetic membrane, in particular the supramolecular organization of different membrane proteins around the RC.[21]

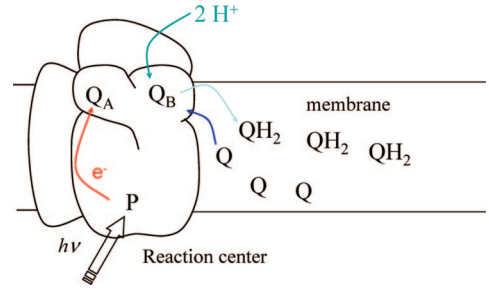

Figure 1. Scheme of the light-induced reaction taking place in a reaction center (RC). P is the primary donor (a dimer of BCHl-*a*), Q_A and Q_B are two ubiquinone molecules inside the RC, and Q and QH_2 represent, respectively, the ubiquinone and ubiquinol molecules in the photosynthetic membrane. Differently from Q_B, Q_A is tightly bound to the RC; it cannot be double reduced to ubiquinol and it cannot change its location.

The internal photochemistry of the RC can be summarized as follows. As can be seen in Figure 1, the absorption of a photon by a special pair of bacteriochlorophyll-*a* molecules, called primary donor P_{870}, leads to the transfer of an electron from P to an electron acceptor Q_A, a ubiquinone molecule. A second ubiquinone molecule, named Q_B, accepts two electrons from Q_A in two successive photochemical events. Both electron transfers from Q_A to Q_B are coupled to a proton uptake from the cytoplasm toward the interior of the protein; the overall result is the formation of an ubiquinol molecule (QH_2).

The formed QH_2 leaves its binding site in the protein to diffuse in the photosynthetic membrane and is replaced by a new ubiquinone molecule coming from the membrane pool of quinones.

Ubiquinol is then reoxidized by another membrane enzyme of the photosynthetic electron transfer chain called cytochrome bc_1 complex. Thanks to the orientation of the RC and of the bc_1 complex in the membrane, the cyclic mechanism of all these redox reactions moves protons from the cytoplasm to the periplasm, thus acting as a light-driven proton pump system. The resultant H^+ gradient is the driving force for the synthesis of ATP, which is used to power the metabolic reactions of the cell.

The Q/QH_2 turnover process is of particular interest since it is the rate-limiting step when multiple ubiquinone reduction is taking place. The protein supramolecular organization in the membrane is particularly important because the architecture of protein assembly within the membrane seems to regulate the diffusion of Q and QH_2 to and from the RC.[21] Time-resolved infrared difference spectroscopy has largely been used in order to investigate the molecular details of photosynthetic reactions.[8−11,22−25] The photoreduction of Q to QH_2 can be monitored in the time scale of rapid-scan FTIR spectroscopy (several hundredths of milliseconds), whereas a protein conformational change associated with the photoreaction takes place at a much shorter time scale.[10] The experimental scheme involves the recording of time-resolved spectra both under illumination (photoaccumulation stage) and after illumination ("relaxation" stage, where external redox mediators bring the system back to its initial states). This approach has been successfully applied to photosynthetic RCs[9] and membranes[10,11] from *Rb. sphaeroides*. In the case of photosynthetic membranes, IR bands for ubiquinol formation inside photosynthetic membranes have been identified (which allow to follow the kinetic of ubiquinol formation), as well as other interesting phenomena, such as

protein conformational changes or phospholipid headgroup perturbation.[10]

Through the analysis of this example, it will be shown how to take into account (1) the specificities of the differential spectroscopic data; (2) the presence of reactions taking place at different time scales; and (3) the treatment of the two different phases found in our experimental approach (i.e., under and after continuous illumination conditions; see below for further details). Five data sets will be analyzed jointly using HS-MCR. They all monitor the same process, but under various experimental conditions. Due to its complexity, this system can be considered an excellent case study to demonstrate that the hard−soft methodology can be applied to analyze time-resolved infrared difference spectra of any light-induced kinetic system.

Experimental Section

Photosynthetic membranes from *Rb. sphaeroides* and samples for FTIR measurements were prepared as described in Clayton et al.[26] and purified by sucrose gradient. Samples for FTIR measurements were prepared by diluting chromatophores to a concentration of 3 μM in RCs in 70 mM Tris buffer (pH 8) and adding 10 μM antimycin and 10 μM myxothiazole as specific inhibitors of the cytochrome bc_1 complex. To avoid contributions arising from the photooxidation of the primary donor P870, 10 mM sodium ascorbate and 20 mM 2,3,5,6-tetramethyl-*p*-phenylenediamine (diaminodurene) were present as external redox components to ensure fast reduction of P_{870}^+. The suspension was centrifuged at 220 000*g* for 15 min and the obtained pellet was squeezed and sealed between two CaF2 windows.

A Bruker IFS 88 FTIR spectrometer equipped with a photoconductive MCT-A detector and a KBr beamsplitter was used. Time-resolved FTIR spectra were recorded under and after continuous illumination of the sample with a 250 W tungsten−halogen lamp (Oriel), using rapid-scan conditions adapted from those described in Mezzetti et al.[10] Before the photochemical reaction was monitored, reference scans were recorded in the dark. 200 interferograms were therefore recorded and then coadded. Fourier transform led to the single beam spectrum S(0) of the initial state. The data set of an experiment is the result from several cycles, ranging in number of accumulations from 150 to 1350 (see later). In each cycle, after the recording of the 200 reference interferograms, five interferograms were recorded (and Fourier transformed) to assess the noise level. Then, the photochemical reaction was triggered by the opening of a mechanical shutter (Uniblitz) connected to the lamp (which remained switched on during the whole duration of the experiment), with the light switched on during 4.3 s. Interferograms were acquired under illumination and averaged in groups of five (duration 217 ms) to monitor the evolution of the sample. Fourier transformation led to a series of single beam spectra $S(t)$, where t is an average value of the 217 ms time window of the measurement time. Then, using the mechanical shutter, the illumination was stopped, and interferograms were acquired and Fourier transformed in the same way to monitor the relaxation of the sample in the dark during 55 s. Again, Fourier transformation led to a series of single beam spectra $S(t)$ taken at a different time in order to follow the slow process of reestablishment of the initial conditions by the external redox mediators (diaminodurene and ascorbate). At the end of the measurement, the system was left several minutes in darkness to allow a complete relaxation before repeating the cycle.

TABLE 1: Different Data Sets Registered on the Same Sample under Different Experimental Conditions

experiment	light intensity in photoexcitation (in % of transmission filter)	no. of accumulations
$\mathbf{D}_{hi}$	8	150
$\mathbf{D}_{med}$	5	750
$\mathbf{D}_{low1}$	2.2	1350
$\mathbf{D}_{low2}$	2.2	1050
$\mathbf{D}_{low3}$	2.2	1050

FTIR difference spectra were calculated from the single-beam spectrum obtained in the dark and the single-beam spectrum obtained at time t according to the formula $\Delta A = -\log(S(t)/S(0))$.

Data Treatment

Data Sets. Five experiments were performed successively on the same sample in different conditions of illumination intensity and number of accumulations. These two experimental factors influence the photochemical process and the signal-to-noise ratio (SNR) of the measurement. Both were modified during the acquisition of the different data sets. Each data set consists of 38 FTIR difference spectra recorded between 1244 and 1784 cm^{-1} at a resolution of 4 cm^{-1} in a global time window of 1 min. Consequently, the dimensions of the experimental data sets are 38 × 281. The first 20 spectra correspond to the first 4.3 s of the experiment; i.e., they were recorded under continuous illumination. They correspond to the excitation of the sample (three transmission filters were used in order to set different levels of light intensity). The following 18 spectra were acquired in the dark to monitor sample relaxation. Five data matrices ($\mathbf{D}_{hi}$, $\mathbf{D}_{med}$, $\mathbf{D}_{low1}$, $\mathbf{D}_{low2}$, and $\mathbf{D}_{low3}$) were obtained from experiments performed under the conditions described in Table 1. The rows are the spectra collected at each time position, and the columns describe the variation of absorbance of the sample at each wavelength.

It should be pointed that the number of accumulations per spectrum has been adapted to the light power in the photoaccumulation stage. Indeed, a progressive "fatigue" of the sample is known to exist in this kind of processes and samples, partly due to sample aging, but mainly to the stress induced by light exposure and by the repetition of the photoreaction.[11] Such an aspect affects the concentration level of the products formed but not the shape of the related pure spectra contributions. To avoid the fatigue effect as much as possible, the experiment under strong exposure to light ($\mathbf{D}_{hi}$ set of data) has been performed at the beginning using a small number of accumulations (150 scans). The experiment under medium light exposure was performed immediately afterward, averaging a medium number of scans (750). Experiments under low light exposure were performed at the end, using a higher number of accumulations (1350 or 1050 scans).

Hybrid Hard and Soft Multivariate Curve Resolution (HS-MCR). Hard−soft multivariate curve resolution (HS-MCR) is an evolution of the soft modeling algorithm multivariate curve resolution-alternating least squares (MCR-ALS) including a hard-modeling constraint.[16−18] The basic MCR-ALS algorithm decomposes a data matrix from an evolving system containing mixed information, **D,** into the product of two small matrices containing the pure concentration and response profiles of the compounds in the system, **C** and $\mathbf{S}^\mathbf{T}$, respectively.[27,28] The bilinear model in eq 1 is in agreement with the Lambert−Beer law

$$\mathbf{D} = \mathbf{C}\mathbf{S}^{\mathbf{T}} + \mathbf{E} \quad (1)$$

When focusing on time-resolved spectroscopic data, $\mathbf{D}(m \times n)$ contains the m measured spectra (at n wavenumbers) ordered as a function of time. $\mathbf{C}(m \times p)$ is formed by columns describing the concentration profiles of the p pure species in the system at m time points and $\mathbf{S}^{\mathbf{T}}(p \times n)$ contains p rows with the related pure spectra. $\mathbf{E}(m \times n)$ is the error matrix containing the residuals. This same bilinear model extends to the simultaneous treatment of several experiments. In this case, the matrix $\mathbf{D}$ is formed by a columnwise augmented matrix (containing submatrices of the different experiments appended one on top of each other [$\mathbf{D}_1$; $\mathbf{D}_2$;...; $\mathbf{D}_n$]) and is decomposed into the product of a columnwise augmented $\mathbf{C}$ matrix (with the submatrices of concentration profiles linked to each experiment [$\mathbf{C}_1$; $\mathbf{C}_2$;...; $\mathbf{C}_n$])) and a matrix $\mathbf{S}^{\mathbf{T}}$, with a single set of pure spectra, valid for all the experiments treated together.

The full MCR-ALS[13] procedure can be summarized in the following steps:

(1) determination of the number of components contributing to $\mathbf{D}$;

(2) construction of initial estimates of the concentration profiles $\mathbf{C}$ using chemical insight or chemometric methods such as evolving factor analysis;[29]

(3) least-squares calculation of $\mathbf{S}^{\mathbf{T}}$ under suitable constraints given $\mathbf{D}$ and $\mathbf{C}$;

(4) least-squares calculation of $\mathbf{C}$ under suitable constraints given $\mathbf{D}$ and $\mathbf{S}^{\mathbf{T}}$, and

(5) reproduction of $\mathbf{D}$ using the product of calculated $\mathbf{C}$ and $\mathbf{S}^{\mathbf{T}}$ in steps 3 and 4;

(6) go back to step 3 until convergence.

The resolved profiles may not be unique, being subject to rotational ambiguities.[13] The use of constraints limits the number of possible solutions and gives chemical meaning to the resolved kinetic and spectroscopic profiles.[27,30−33] Constraints can be defined as any mathematical or chemical property that concentration profiles and/or spectra must obey. In the MCR-ALS algorithm, the least-squares calculated profiles in $\mathbf{C}$ and $\mathbf{S}^{\mathbf{T}}$ are modified so that they fulfill the suitable constraints. All constraints can be applied in an optional and different way to $\mathbf{C}$ and $\mathbf{S}^{\mathbf{T}}$ (and the submatrices therein) and to each of the profiles in these matrices. For time-resolved differential FTIR spectroscopic data, suitable constraints could be nonnegativity in the concentration direction and unimodality (only one maximum in the profile) for the kinetic profiles expected to have a growth−decay shape. Since the difference spectra recorded may have positive and negative values, the $\mathbf{S}^{\mathbf{T}}$ matrix should be left unconstrained.

The main difference between MCR-ALS and its variant HS-MCR is the inclusion of kinetic models as an additional constraint to model the shape of the concentration profiles.[16] Thus, in step 4, the concentration profiles in $\mathbf{C}$ (all or only some of them) are used as input of a nonlinear kinetic fitting. Then, the fitted profiles update the initial soft-modeled ones and the rate constants are obtained as additional information. Keeping the flexibility of the basic MCR-ALS algorithm in the introduction of constraints, the different experiments may be fitted using a global kinetic model[34] or individual kinetic models. Besides, the introduction of the hard-modeling constraint greatly decreases the rotational ambiguity linked to the classical soft-modeling MCR-ALS approach.

In the context of the presented example, there are several advantages connected with the use of HS-MCR to model time-resolved FTIR difference spectra:

(a) The possibility to model a kinetic process in the presence of absorbing interferences that do not follow a kinetic model.[17] This advantage comes from the fact that not all the profiles in the $\mathbf{C}$ matrix need to be included in the nonlinear kinetic fitting. This allows soft modeling of species related to events that do not follow a clear model or that happen too fast as compared with the time scale of the experiment (e.g., a too fast protein conformational change);

(b) The possibility to use kinetic models including transparent species to deal with the specificities of difference spectra. This aspect of the methodology has been extensively described by the authors in a previous paper and the reader is sent to this reference to understand the details linked to the kinetic model fitting.[12] As a way of example, in a photochemical reaction A $\rightarrow$ B monitored by difference spectroscopy, only one absorbing contribution is detected that evolves with a concentration profile equal in shape to $\mathbf{c}_B$ (the concentration profile of species B in the kinetic model) and a pure spectrum corresponding to ($\mathbf{s}_B - \mathbf{s}_A$), i.e., the pure spectra of B minus the pure spectra of A. Therefore, the original kinetic model A $\rightarrow$ B should be preserved to describe properly the behavior of the absorbing contribution, but the species A should be set as a "nonabsorbing" species because no measurable signal can be associated with it. To summarize it for a general case, the initial species in difference spectroscopy should be taken into account and be incorporated as nonabsorbing species to be able to postulate a realistic kinetic model of the monitored events;[17]

(c) The possibility to perform simultaneous analysis of several experiments and fit different kinetic models to them. This fact will help to account for mechanism changes in the photochemical process coming from the variation of illumination intensity used in the different experiments. Moreover, the general benefit of analyzing several experiments together should not be overlooked. The amount of information handled together when using a columnwise augmented data set reduces significantly the rotational ambiguity linked to the resolution process and improves significantly the quality of the final results obtained.

Finally, a novel point in the implementation of the HS-MCR algorithm needs to be stressed because it relates to the peculiar nature of the experimental scheme used here, often applied in photochemical process monitoring. Each experiment is divided into two phases: (1) excitation and (2) relaxation of the sample, followed under the action of light and in darkness, respectively. Within each experiment, both phases follow opposite kinetic models that should be fitted separately. At the same time, these phases are intimately connected and the evolution of the relaxation phase depends on the final conditions reached by the sample in the excitation phase, which cannot be known a priori from the sole information contained in the raw data. A modification in the implementation of the kinetic constraint in HS-MCR has been performed so that the kinetic fitting can be carried out sequentially for the photoexcitation and relaxation phases of the process. Thus, in each iteration, the first step is the kinetic fitting of the photoexcitation phase of each experiment, for which the necessary information of initial concentrations and estimate of rate constants is available. As a result, the related rate constants are obtained and the concentrations at the end of the excitation phase of each process contribution. Now, the kinetic fitting of the relaxation phase of each experiment can be carried out taking as initial concentrations of the contributions the concentrations values at the end of the excitation. The successive iterations improve the resolution integrating the information available in both phases until the final result is obtained.

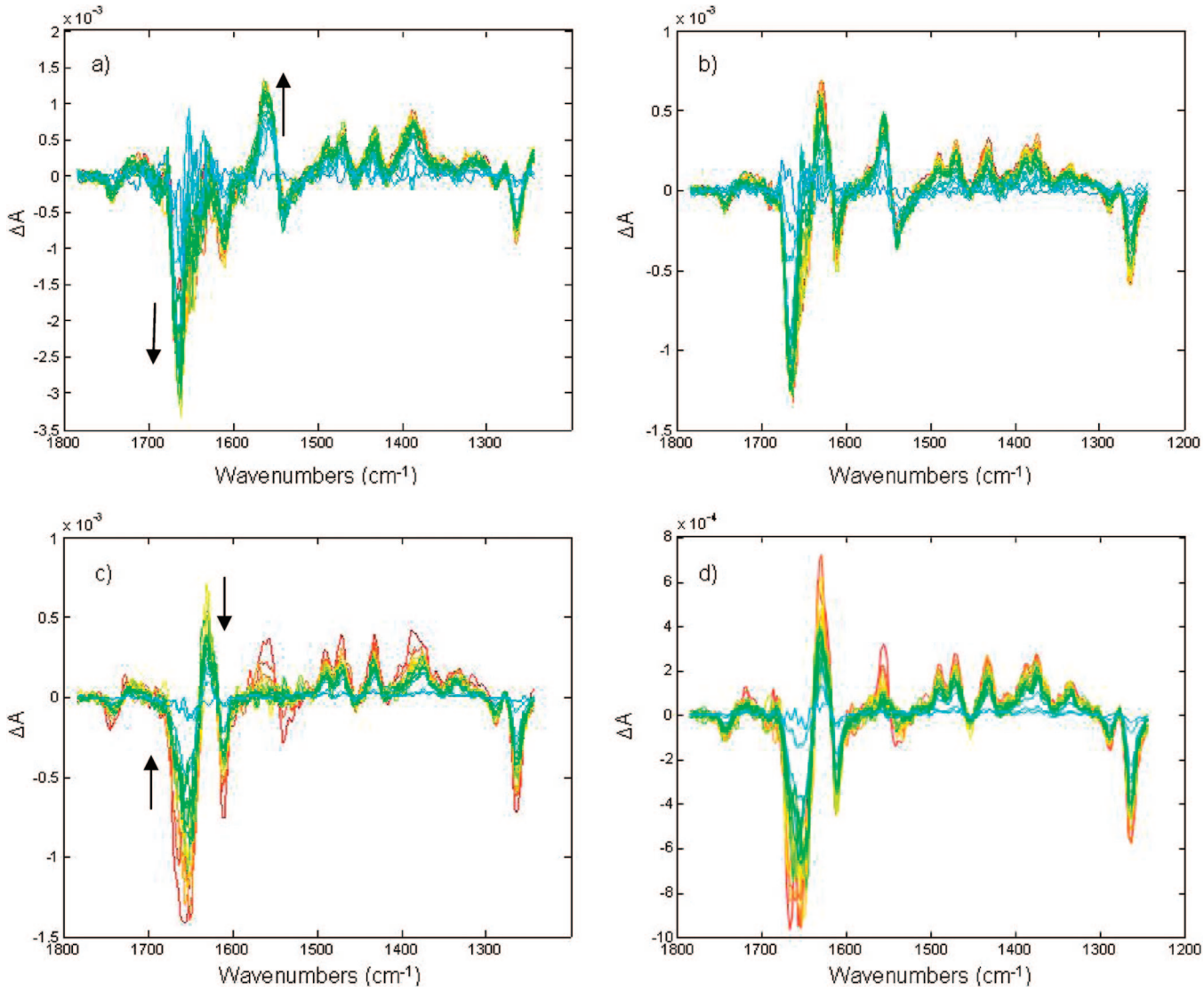

Figure 2. Plots of the difference FTIR spectra acquired during the 4.3 s excitation phase of the RC of *Rhodobacter sphaeroides* for two light intensities (a) $\mathbf{D}_{hi}$ and (b) $\mathbf{D}_{low1}$, and corresponding relaxation phases (c) $\mathbf{D}_{hi}$ and (d) $\mathbf{D}_{low1}$. Spectra are color coded from blue to red as a function of the excitation of the sample. The arrows indicate the direction of evolution.

The algorithm HS-MCR has been programmed by the authors under MATLAB environment and is available on request. The soft-modeling MCR-ALS code is provided with a graphical user interface and can be downloaded for free at the web page: www.ub.edu/mcr/.

Results and Discussion

Difference absorbance spectra recorded during some rapid-scan FTIR experiments on the photosynthetic membranes of *Rb. sphaeroides* are shown in Figure 2. They correspond to the excitation phase of $\mathbf{D}_{hi}$ and $\mathbf{D}_{low1}$. A first look at the untreated raw spectra can already give some interesting pieces of information. The main observation is the emergence, during the photoaccumulation period, of difference absorbance bands, in particular at 1566 (+), 1539 (−), 1491 (+), 1471 (+), 1433 (+), 1385 (+), 1375 (+), 1288 (−), and 1263 (−) cm^{-1}. Positive bands in difference spectra are related to the emergence of products, whereas negative bands account for the disappearance of reactants in a process. The negative band at 1263 cm^{-1} arises from the C−O−C modes of the methoxy groups of ubiquinone.[35] This band is particularly interesting because it is usually taken as an indicator of the consumption of ubiquinone molecules.[10,22] The evolution of the bands during the relaxation stage is the opposite and the disappearance of the bands is the phenomenon monitored. Some differences can also be observed between the two experiments presented in Figure 2 because of the different experimental conditions, the main aspect being that the intensity of the light in the excitation period has a strong influence on the global evolution of the raw spectra collected. This may indicate that different chemical species and/or different chemical reactions are involved in the overall process. As can be expected, light influences the rate constants of photoinduced Q reduction.

In all the following data treatment, the amide I band region (corresponding to the 1680−1580 cm^{-1} spectral range) will be excluded from the data sets treated due to the high noise level. Indeed, the experimental noise in this spectral range is roughly 5 times more intense than elsewhere. Besides, the information in the amide I band region is not the most relevant in the explanation of the $Q \rightarrow QH_2$ process because the most specific spectral features of these species are linked to smaller bands at both sides of this main band. Nevertheless, the pure spectra in the original full spectral range can be recovered via a single least-squares step based on the bilinear model in eq 1, using

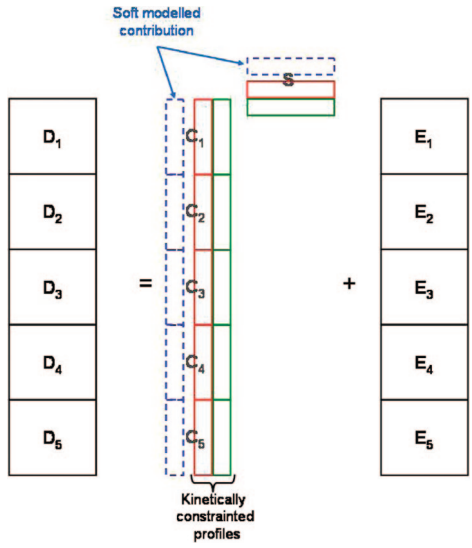

Figure 3. Scheme of the columnwise augmented matrix [$\mathbf{D}_{hi}$; $\mathbf{D}_{med}$; $\mathbf{D}_{low1}$; $\mathbf{D}_{low2}$; $\mathbf{D}_{low3}$] and constraints applied for global hard−soft multivariate curve resolution.

the full raw data set **D** (including the amide I band), and the **C** matrix obtained from the resolution of the data set with the Amide I band region excluded.

A soft-modeling analysis of time-resolved FTIR difference spectra of the same photobiological system has been reported in a previous paper, working with experiments that did not reach the maximum illumination intensity used in this work.[11] On that ground, it was decided, as a first step, to perform a new soft-modeling analysis on the set of data ($\mathbf{D}_{hi}$, $\mathbf{D}_{med}$, $\mathbf{D}_{low1}$, $\mathbf{D}_{low2}$, and $\mathbf{D}_{low3}$) to get a more complete overview of the events concurring on the light-induced kinetic system. The different data sets have been arranged in an augmented matrix, as presented in Figure 3. The rank estimations have been based on previous study performed by MCR-ALS[11] and on the analysis of the augmented data sets using evolving factor analysis for rank-deficient matrices.[36] This step is not described here for purpose of brevity. The conclusions drawn show that three distinct contributions are present.

A purely soft model explaining 93% of the variance was then constructed (see Supporting Information). It permits to conclude that the light (during 4.3 s) or darkness conditions correspond to opposite processes as expected. This makes sense, because when the light is switched on, the light-driven ubiquinone reduction to ubiquinol goes in one way, whereas when the light is off the reaction goes backward because of the action of the redox mediators. This confirms the need of using opposite kinetic models to fit the two phases of each experiment. A more interesting point is that light intensity seems to change the reactional scheme. Previous results[10,11] showed that two common contributions could be found in all experiments and were linked to a "fast" process (i.e., a process that takes place very quickly after beginning of the illumination period and disappears very quickly after the end of the light exposure, in a time scale shorter than some hundredths of milliseconds, attributed to a protein conformational change) and a "slow" process (a reaction that can be fitted with a first order kinetic model both during the illumination period and the "relaxation" period, associated with the ubiquinone/ubiquinol transformation). In the present soft-modeling analysis, the presence of a third contribution, only present at medium or high illumination intensities, has been confirmed, the spectral contribution of which seems to relate to a different ubiquinone/ubiquinol transformation.

TABLE 2: Kinetic Models Implemented on the Five Data Sets during the HS-MCR Resolution

data sets	excitation	relaxation
$\mathbf{D}_{hi}$	soft-modeled species	
	$Q \rightarrow QH_2$	$QH_2 \rightarrow Q$
	$Q' \rightarrow QH_2'$	$QH_2' \rightarrow Q'$
$\mathbf{D}_{med}$	soft-modeled species	
	$Q \rightarrow QH_2$	$QH_2 \rightarrow Q$
	$Q' \rightarrow QH_2'$	$QH_2' \rightarrow Q'$
$\mathbf{D}_{low1}$	soft-modeled species	
	$Q \rightarrow QH_2$	$QH_2 \rightarrow Q$
$\mathbf{D}_{low2}$	soft-modeled species	
	$Q \rightarrow QH_2$	$QH_2 \rightarrow Q$
$\mathbf{D}_{low3}$	soft-modeled species	
	$Q \rightarrow QH_2$	$QH_2 \rightarrow Q$

The soft-modeling results provide a good preliminary view of the system that was used to propose thee kinetic models and analysis conditions for the definitive application of HS-MCR. Since HS-MCR improve substantially the quality of the final results (i.e., rotational ambiguity is dramatically decreased) and the knowledge of the chemical system, the interpretation of the spectral nature of these contributions and the final conclusions about the study of this photochemical problem will be extracted from the application of this data treatment.

As previously said, HS-MCR offers a solution to the dilemma of the simultaneous presence of contributions that can be described by a kinetic model and others that cannot. In this example, the concentration profile of the fast contribution linked to the protein conformational change will be modeled using soft-modeling constraints (nonnegativity), whereas the concentration profiles of the two other contributions, potentially linked to ubiquinone (Q)/ubiquinol (QH_2) transformations will be set to respect a kinetic model. In view of the soft-modeling results obtained, we have proposed kinetic models that fulfill the rank estimation obtained; i.e., one or two contributions can be subject to kinetic fitting. We have also opted for the simplest possible model that seems to indicate two possible ways of ubiquinol formation. Models for different number of components or formally more complex did not improve significantly either the variance explained or the interpretability of the results. Table 2 shows the analysis conditions and the set of kinetic models for every phase of the five experiments. Thus, for all experiments, a contribution obeying the kinetic model $Q \rightarrow QH_2$ (in the photoaccumulation phase), and $QH_2 \rightarrow Q$ (in the relaxation phase) is proposed, whereas experiments performed in medium and strong illumination conditions have an additional contribution obeying the models $Q' \rightarrow QH_2'$ (in the photoaccumulation phase), and $QH_2' \rightarrow Q'$ (in the relaxation phase).

Figures 4 and 5 present the resolved spectra and concentration profiles obtained by HS-MCR from the simultaneous analysis of the five experiments performed, respectively. The rate constants obtained from the kinetic fittings are in Table 3. The error associated with the rate constants comes from the application of the Levenberg−Marquardt algorithm in the kinetic fitting step of HS-MCR.[37] The data variance explained with this analysis is 92.4%, which is satisfactory for this kind of measurements. The very low decrease in variance explained as compared with the pure soft-modeling MCR-ALS (93% without any model assumption) supports the validity of the kinetic model postulated. However, this validity should be confirmed by the interpretability of the concentration profiles and spectra obtained. As expected, three contributions are modeled: the soft-modeled

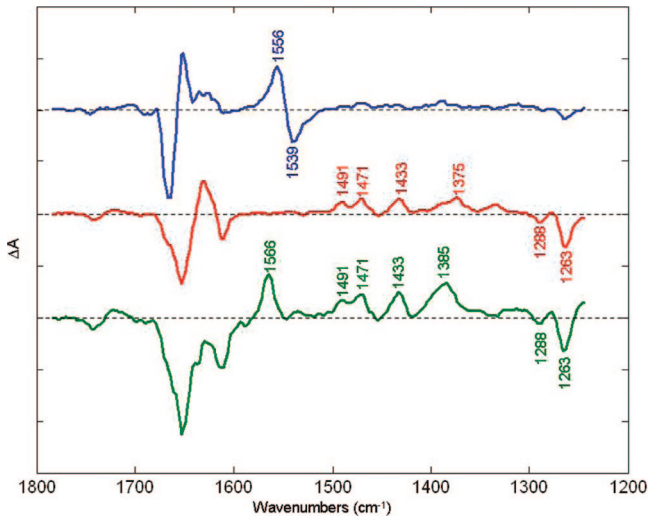

Figure 4. Plots of the resolved spectra obtained from HS-MCR. The protein contribution is in blue, and in red and in green the two processes involving the formation of ubiquinol (QH_2).

contribution (in blue) and two contributions forced to obey kinetic models, one common to all experiments (in red) and one present only in the experiments with medium or strong illumination conditions (in green).

It is important to underline that the concentration profile of the soft-modeled contribution (in blue) behaves identically in the five experiments. As soon as the illumination begins, the concentration profile increases quickly and reaches a maximum. Once the light is switched off, it decreases quickly to zero. The most informative peaks of the resolved difference spectrum are labeled in Figure 4. This contribution is mainly identified by positive and negative peaks at 1556 and 1539 cm^{-1}, in the so-called amide II region. Intense spectral contributions are visible also in the amide I region, at 1651 and 1664 cm^{-1}. This region is more informative, but also less reliable because of the noise influence. The simultaneous presence of the bands mentioned above is a sign that can be interpreted as a protein conformational change.

As stated before, the concentration profiles of the other two contributions are constrained by kinetic models. The efficient strategy connecting the excitation and relaxation models can be seen in the continuous evolution of the concentration profiles from the photoaccumulation to the relaxation phase. Below, we explain in detail the meaning of the kinetic profiles and spectra corresponding to these two contributions.

The resolved difference spectrum of the second contribution (present in all the spectral data sets and shown in red in Figure 4) is characterized by the peaks of ubiquinol formation (positive bands) and ubiquinone consumption (negative bands). More in detail, the 1491, 1471, 1433, and 1388 cm^{-1} positive bands have been identified as arising from ubiquinol vibrations.[10] Similar band patterns have been assigned to ubiquinol in solution[38] and other biological systems.[39] Characteristic bands of ubiquinone consumption are visible as negative peaks at 1611, 1288, and 1263 cm^{-1}.[10] Therefore, the kinetic profile of this contribution clearly shows the ubiquinone reduction to ubiquinol under the light excitation and the opposite process during the relaxation of the system. In experiments under low illumination, $\mathbf{D}_{low1}$, $\mathbf{D}_{low2}$, and $\mathbf{D}_{low3}$, the rate constants are comparable in both the photoaccumulation and relaxation stage. This reflects the similarity of the experimental conditions in the three batches. Yet, a small loss of efficiency of the photochemical process agreeing with the sequence of execution of the experiments can be observed, as reported previously.[11] This is attributed to a gradual degradation of the biological sample after long periods of illumination. A slight evolution in the value of the rate constant, k_1, is also visible, being higher in $\mathbf{D}_{med}$ than in $\mathbf{D}_{low1}$, $\mathbf{D}_{low2}$, and $\mathbf{D}_{low3}$. This tendency is not consistent in $\mathbf{D}_{hi}$, where the dominance of the third contribution may likely influence the development of the kinetic process linked to the second contribution. The most relevant observation is that, although being a photoinduced process, the production of ubiquinol described by this second contribution does not increase proportionally to the illumination power, as can be easily seen by comparing the decreasing magnitude of the kinetic profiles when passing from $\mathbf{D}_{low1}$, $\mathbf{D}_{low2}$, and $\mathbf{D}_{low3}$ to $\mathbf{D}_{med}$ and $\mathbf{D}_{hi}$. This can be explained by the presence of the third contribution of the photochemical system.

In fact, the spectrum of the third contribution (in green in Figure 4) shows also positive bands characteristic of ubiquinol formation (at 1491, 1471, 1433 cm^{-1}) and negative bands linked to ubiquinone consumption (at ~1611, 1288, 1263 cm^{-1}). This fact supports that the third contribution may also represent a light-induced ubiquinol formation process. However, this new process seems to be different from the one described by the second contribution, not only for the kinetics and the conditions under which it is observed, but also for the spectral features of the resolved difference spectrum. In the spectrum of this third contribution, a strong positive band is observed at 1566 cm^{-1}, whereas the second contribution did not show any peak in this region. Several differences between the spectra of the second and the third contribution can also be seen in the 1680−1580 cm^{-1} and in the 1410−1300 cm^{-1} ranges. The kinetic profiles indicate that the process responsible for the third contribution only appears under strong light excitation conditions (in $\mathbf{D}_{med}$ and $\mathbf{D}_{hi}$), and has a tendency to replace the main process observed at low illumination intensities. Indeed, the increasing prevalence of the third contribution is seen looking more in detail at the kinetic profiles of $\mathbf{D}_{low1}$, $\mathbf{D}_{low2}$ and $\mathbf{D}_{low3}$, where this contribution is absent, of $\mathbf{D}_{med}$, where the two ubiquinone/ubiquinol processes compete and, finally, of $\mathbf{D}_{hi}$ where the third contribution becomes clearly predominant. This is coherent with the value of the calculated rate constants k_2 and k_4 which fit the excitation and relaxation phases for the third contribution.

It is important to note that this third contribution was also detected in the soft-modeled analysis presented here and in the previous study mentioned.[11] However, the combined use of experiments obtained under stronger light conditions, where this third contribution becomes a major part of the signal measured, and the hybrid hard- and soft-modeling procedure, where the rotational ambiguity affects in a much lower extent the results obtained, has allowed for a significant improvement in the definition of the structure and kinetics of this contribution as compared with the previous soft-modeling study.[11] A detailed interpretation of this third contribution is beyond the scope of this paper and would require experiments in different conditions (e.g., in D_2O solution, investigation of the influence of temperature, use of membranes from genetically modified bacteria). Yet, it is important to mention that the recovered spectrum and kinetic profile seems now to exclude a previous tentative interpretation (i.e., oxidation of external chemical mediators).[11]

It is worth noticing that the present results showing the presence of two contributions (the second, red, and the third, green, shown in Figure 4) both representing (at least partially)

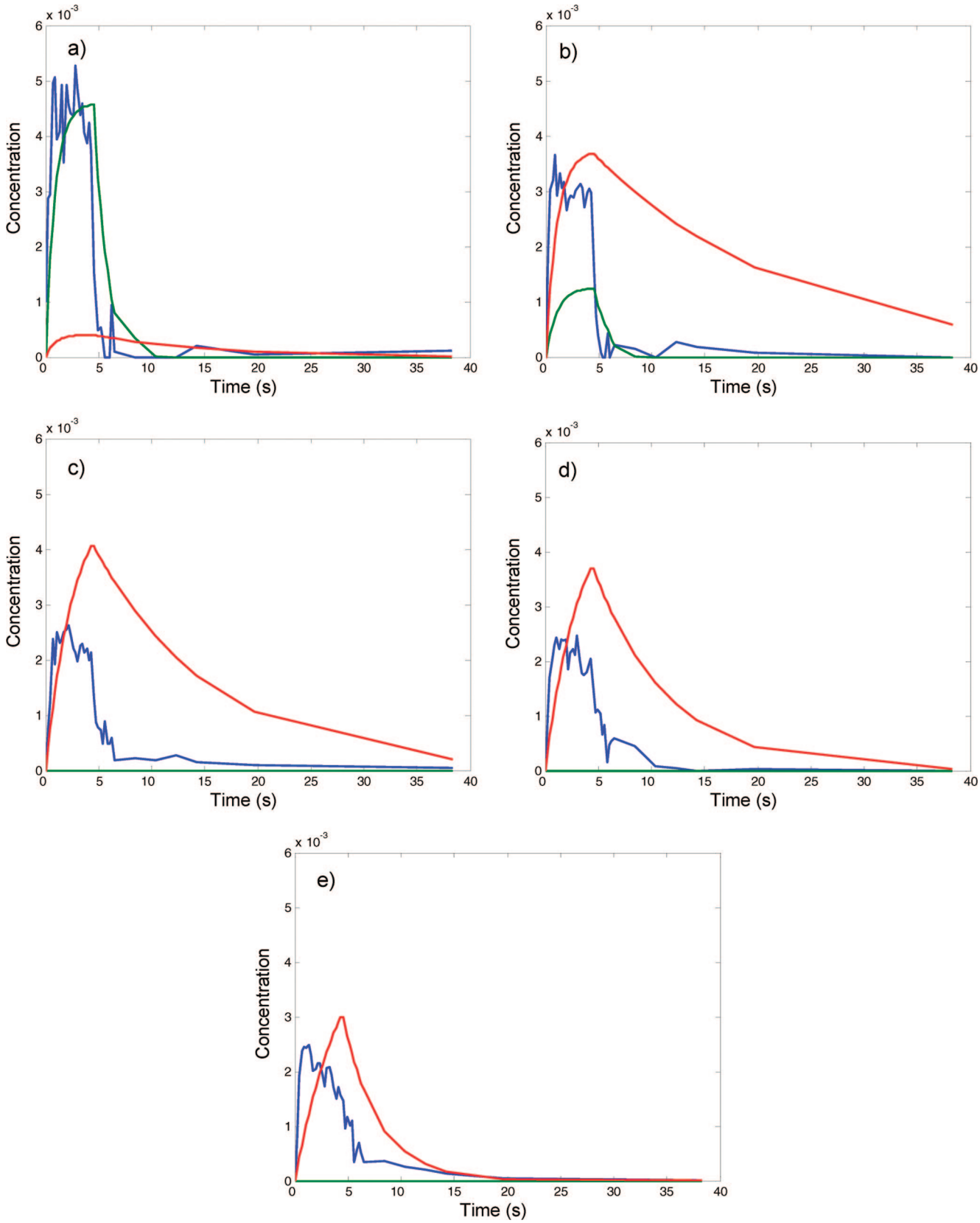

Figure 5. Resolved concentration profiles obtained from HS-MCR for (a) $\mathbf{D}_{hi}$, (b) $\mathbf{D}_{med}$, (c) $\mathbf{D}_{low1}$, (d) $\mathbf{D}_{low2}$, and (e) $\mathbf{D}_{low3}$. The protein contribution is in blue, and in red and in green the two processes involving the formation of ubiquinol (QH_2).

photoinduced ubiquinone reduction to ubiquinol would be consistent with the existence of two somehow different ubiquinone pools in the membrane that would conduct to the ubiquinol formation in different ways. Indeed, it has been noticed in recent papers[40,41] that a considerable fraction of the quinone pool is retained in the so-called "RC protein supercomplex" (a supramolecular aggregate of membrane proteins) even after biochemical extraction. This would be

TABLE 3: Rate Constants Calculated on the Five Data Sets by the HS-MCR Resolution

	excitation		relaxation	
data sets	k_1 (s^{-1})	k_2 (s^{-1})	k_3 (s^{-1})	k_4 (s^{-1})
$\mathbf{D}_{hi}$	0.09 ± 0.02	1.06 ± 0.08	0.09 ± 0.01	0.82 ± 0.01
$\mathbf{D}_{me}$	0.73 ± 0.05	0.25 ± 0.03	0.05 ± 0.01	0.69 ± 0.01
$\mathbf{D}_{low1}$	0.39 ± 0.01	−	0.09 ± 0.01	−
$\mathbf{D}_{low2}$	0.31 ± 0.01	−	0.14 ± 0.01	−
$\mathbf{D}_{low3}$	0.22 ± 0.01	−	0.29 ± 0.04	−

in agreement with the existence of a subpool of quinones internal to the supercomplex (the remaining fraction being external to it) that could react differently from the "external" pool. Nevertheless, further experiments are required to clarify this issue and other interpretations cannot be ruled out.

Conclusion

The analysis of time-resolved infrared difference spectra monitoring photoinduced biochemical processes remains a challenging topic. Indeed, this kind of data presents some specific difficulties, linked to the intrinsic nature of the difference spectra collected and to the presence of concurrent events on the global photochemical process that may differ significantly in mechanism and time scale. Pure hard-modeling approaches, potentially useful to model kinetic processes, fail in the presence of interferences. In these photoinduced processes, the concept of interference extends to any signal contribution that cannot be fitted by a kinetic model, i.e., an inert absorbing compound and, most importantly, species involved in events that take place much faster or much slower than the time scale of the spectroscopic technique used.

A hybrid hard−soft-modeling method, HS-MCR, has been proposed to overcome these limitations. HS-MCR has provided the advantages of combining hard modeling to describe contributions linked to events that can be described by a kinetic model and soft modeling for events that take place out of the time scale used in the spectroscopic technique, e.g., the too fast first contribution in the example presented. The flexibility of HS-MCR has allowed the simultaneous treatment of experiments performed under different conditions of illumination and, therefore, behaving according to different mechanisms or following the same mechanism at different rates. In all these experiments, the suitable kinetic model could be applied and related rate constants were obtained. The modification of HS-MCR to allow for a sequential fitting of the photoexcitation and relaxation phases of the photochemical process has overcome the difficulty linked to the lack of knowledge linked to the initial conditions, i.e., concentrations, at the beginning of the relaxation phase.

All these advantages have been proven to be very useful in the analysis of rapid scan FTIR difference spectra monitoring the photoreduction of the quinone pool in photosynthetic membranes from *Rhodobacter sphaeroides*. The previous interpretation of the reaction mechanism by pure soft-modeling approaches has been significantly enhanced, leading to the characterization of two competing processes under conditions of medium and strong illumination. Moreover, the possibility of obtaining accurate kinetic parameters has allowed investigating other aspects, such as the influence of light intensity on the reaction rate and on the biological degradation. This kinetic information has been obtained in the presence of an interfering contribution to the signal recorded, linked to a protein conformational change, too fast to be hard-modeled at the working time scale used.

The example presented is a case study that clearly shows all the benefits that may be taken from the most recent progress in the HS-MCR method. It is very relevant to stress that the presented methodology is, by no means, restricted to biochemical photoinduced processes, but can be extended to the study of any photoinduced process of environmental or industrial interest.

Acknowledgment. L.B. acknowledges a Ph.D. scholarship from the Ministère délégué à l'Enseignement supérieur et à la Recherche. The Programme Hubert Curien (Picasso 13521SL) is thanked for the international mobility grant provided to L.B., C.R., J.P.H., and A.d.J. L.B. and A.d.J. thank the Spanish government for the financial help linked to the project CTQ2006-15052-C02. The authors thank Dr. Winfried Leibl for help in the FTIR measurements and fruitful discussion. A.M. acknowledges partial financial support from the CEA.

Supporting Information Available: A short description of the rank estimations is provided. This aspect of the work is based on previous study performed by MCR-ALS and on the analysis of the augmented data sets using evolving factor analysis for rank-deficient matrices. This material is available free of charge via the Internet at http://pubs.acs.org.

References and Notes

(1) Albini, A. In *Methods and Reagents for Green Chemistry*; Tundo, P., Perosa, A., Zecchini, F., Eds.; Wiley: New York, 2007; pp 65−75.
(2) Rabek, J. F. *Polymer Photodegradation—Mechanisms and experimental methods*, 1st ed.; Chapman & Hall: London, 1994.
(3) Jaeger, R. C. *Introduction to Microelectronic Fabrication*; Pearson Education Ltd.: Upper Saddle River, NJ, 2001.
(4) Björn, L. O. *Photobiology. The science of Life and Light*, 2nd ed.; Springer: Dordrecht, The Netherlands, 2008.
(5) Braiman, M. S.; Ahl, P. L.; Rotschild, K. J. *Proc. Natl. Acad. Sci. U.S.A.* **1987**, *84*, 5221–5225.
(6) Uhmann, W.; Becker, A.; Taran, C.; Siebert, F. *Appl. Spectr.* **1991**, *45*, 390–397.
(7) Gerwert, K. In *Infrared and Raman spectroscopy of Biological Materials*; Gremlich, H. U., Yan, B., Eds.; Marcel Dekker: New York, 2000; Vol. 24.
(8) Thibodeau, D. L.; Nabedryk, E.; Hienerwadel, R.; Lenz, F.; Mantele, W.; Breton, J. *Biochim. Biophys. Acta, Bioenerg.* **1990**, *1020*, 253–259.
(9) Mezzetti, A.; Leibl, W. *Eur. Biophys. J.* **2005**, *34*, 921–936.
(10) Mezzetti, A.; Leibl, W.; Breton, J.; Nabedryk, E. *FEBS Lett.* **2003**, *537*, 161–165.
(11) Blanchet, L.; Mezzetti, A.; Ruckebusch, C.; Huvenne, J. P.; de Juan, A. *Anal. Bioanal. Chem.* **2007**, *387*, 1863–1873.
(12) Blanchet, L.; Ruckebusch, C.; Huvenne, J. P.; de Juan, A. *Chemom. Intell. Lab. Syst.* **2007**, *89*, 26–35.
(13) Tauler, R. *Chemom. Intell. Lab. Syst.* **1995**, *30*, 133–146.
(14) Navea, S.; de Juan, A.; Tauler, R. *Anal. Chem.* **2003**, *75*, 5592–5601.
(15) Ruckebusch, C.; Duponchel, L.; Huvenne, J. P.; Saurina, J. *Anal. Chim. Acta* **2004**, *515*, 183–190.
(16) de Juan, A.; Maeder, M.; Martinez, M.; Tauler, R. *Chemom. Intell. Lab. Syst.* **2000**, *54*, 123–141.
(17) Amigo, J. M.; de Juan, A.; Coello, J.; Maspoch, S. *Anal. Chim. Acta* **2006**, *567*, 236–244.
(18) Amigo, J. M.; de Juan, A.; Coello, J.; Maspoch, S. *Anal. Chim. Acta* **2006**, *567*, 245–254.
(19) Ermler, U.; Fritzsch, G.; Buchanan, S. K.; Michel, H. *Structure* **1994**, *2*, 925–936.
(20) Okamura, M.; Paddock, M.; Graige, M. S. *Biochim. Biophys. Acta* **2000**, *1458*, 148–163.
(21) Verméglio, A.; Joliot, P. *Biochim. Biophys. Acta, Bioenerg.* **2002**, *1555*, 60–64.
(22) Mezzetti, A.; Nabedryk, E.; Breton, J.; Okamura, M.; Paddock, M.; Giacometti, G.; Leibl, W. *Biochim. Biophys. Acta, Bioenerg.* **2002**, *1553*, 320–330.
(23) Remy, A.; Gerwert, K. *Nat. Struct. Biol.* **2003**, *10*, 637–644.
(24) Mezzetti, A.; Seo, D.; Leibl, W.; Sakurai, H.; Breton, J. *Photosynth. Res.* **2003**, *75*, 161–169.
(25) Bandaranayake, K. M. P.; Wang, R.; Johnson, T. W.; Hastings, G. *Biochemistry* **2006**, *45*, 12733–12740.

(26) Clayton, R. K.; Wang, R. T. *Methods Enzymol.* **1971**, *23*, 696–704.
(27) de Juan, A.; Tauler, R. *Anal. Chim. Acta* **2003**, *500*, 195–210.
(28) Windig, W.; Stephenson, D. A. *Anal. Chem.* **1992**, *64*, 2735–2742.
(29) Maeder, M. *Anal. Chem.* **1987**, *59*, 527–530.
(30) Tauler, R.; Smilde, A.; Kowalski, B. *J. Chemom.* **1995**, *9*, 31–58.
(31) Gemperline, P. *J. Anal. Chem.* **1999**, *71*, 5398–5404.
(32) Tauler, R. *J. Chemom.* **2001**, *15*, 627–646.
(33) Vosough, M.; Mason, C.; Tauler, R.; Jalali-Heravi, M.; Maeder, M. *J. Chemom.* **2006**, *20*, 302–310.
(34) Mas, S.; De Juan, A.; Lacorte, S.; Tauler, R. *Anal. Chim. Acta* **2008**, *618*, 18–28.
(35) Breton, J.; Burie, J.-R.; Berthomieu, C.; Berger, G.; Nabedryk, E. *Biochemistry* **1994**, *33*, 4953–4965.
(36) de Juan, A.; Navea, S.; Diewok, J.; Tauler, R. *Chemom. Intell. Lab. Syst.* **2004**, *70*, 11–21.
(37) Maeder, M.; Neuhold, Y. M. *Practical data analysis in chemistry*; Elsevier: Amsterdam, 2007.
(38) Iwaki, M.; Osyczka, A.; Moser, C.; Dutton, P. L.; Rich, P. R. *Biochemistry* **2004**, *43*, 9477–9486.
(39) Hellwig, P.; Barquera, B.; Gennis, R. B. *Biochemistry* **2001**, *40*, 1077–1082.
(40) Comayras, F.; Jungas, C.; Lavergne, J. *J. Biol. Chem.* **2005**, *280*, 11203–11213.
(41) Francia, F.; Dezi, M.; Rebecchi, A.; Mallardi, A.; Palazzo, G.; Melandri, B. A.; Venturoli, G. *Biochemistry* **2004**, *43*, 14199–14210.

JP8056042